Optical Spectroscopy of Candidates of Young Stellar Objects in NGC 1333

Yoichi Itoh[1], Ranjan Gupta[2], Yumiko Oasa[3], Asoke Sen[4],
Munechika Tanaka[1], Tsuyoshi Terai[1], and Seina Nakaoka[1]
[1]*Graduate School of Science, Kobe University, 1-1 Rokkodai, Nada, Kobe 657-8501*
yitoh@kobe-u.ac.jp
[2]*Inter University Centre for Astronomy and Astrophysics, Ganeshkhind, Pune 411 007, India*
[3]*Faculty of Education, Saitama University, 255 Shimo-Okubo, Sakura, Saitama, Saitama*
[4]*Department of Physics, Assam University, Silchar 788 001, India*

(Received 2000 December 31; accepted 2001 January 1)

Abstract

We carried out low-resolution optical spectroscopy of 14 low-luminosity young stellar object (YSO) candidates in the NGC 1333 cluster. These objects were previously identified by the near-infrared imaging survey. Eleven objects were confirmed as YSOs by the Hα line emission. Strengths of the Hα emission are correlated with the near-infrared excesses of the objects. Spectral types of all YSOs are estimated to be M-type, indicative of low-mass. Comparisons of the results of our spectroscopic observations and the previous photometric observations with evolutionary tracks on the HR diagram suggest two objects to be young brown dwarfs.

Key words: stars: formation; pre-main sequence; low-mass, brown dwarfs

1. Introduction

Various observational studies have revealed rich populations of young very-low mass stars and young brown dwarfs in many star-forming regions. It is generally considered that they are born in the similar way that a solar-mass star is; they are born in a molecular cloud core then evolve with accretion and outflow phenomena. Jayawardhana et al. (2003) found strong Hα line emissions of accretion origin in the spectra of young brown dwarfs. They indicated that the accretion rate of young brown dwarfs is lower than that of solar-mass YSOs. Whelan et al. (2005) detected broad Hα emission line and blue-shifted forbidden emission lines associated with a young brown dwarf, ρ Oph 102, both of which indicate an outflow activity.

These accretion and outflow phenomena are closely related to presence of a circumstellar disk. Luhman et al. (2005) observed a less-massive brown dwarf, OTS 44 originally discovered by Oasa et al. (1999), with the Spitzer Space Telescope. By constructing its spectral energy

distribution, they claimed that the object exhibits strong infrared excess. Their conclusion that OTS 44 has a circumstellar disk is a natural consequence, since the object was identified as a YSO originally by its near-infrared excess (Oasa et al. 1999). Based on the intrinsic near-infrared excesses, near-infrared imaging surveys have identified many candidates of young very-low mass stars and young brown dwarfs in many star-forming regions (e.g., Comeron et al. 1993, Itoh et al. 1996, Oasa et al. 1999).

The NGC 1333 cluster is one of the nearest intermediate-mass star forming regions. It is a part of the Perseus molecular cloud. Oasa et al. (2008) carried out near-infrared imaging survey of a $5' \times 5'$ region of NGC 1333. The field of view contained SVS 13, an active outflow source. They detected 76 objects, about half of which show near-infrared excesses. Among them, several tens of faint objects are estimated to be substellar-mass objects.

In this paper, we present the results of a low-resolution optical spectroscopy of the faint YSO candidates in the NGC 1333 cluster. We confirm their YSO nature by detecting the Hα emission line. We also determine optical spectral types, thus masses and ages, of the YSOs. As in Oasa et al. (2008) we adopt the distance of 320 pc to the cluster here.

2. Observations and Data Reduction

Ten objects were selected as the primary targets of the spectroscopic observations. All objects are previously identified as the YSO candidates by Oasa et al. (2008) or Aspin et al. (1994) (Table 1). The sample of the primary targets is nearly flux-limited. By rotating the instrument, we also took spectra of four secondary targets which are located close to the primary targets. In this case, the spectra of the primary targets and the secondary targets were taken simultaneously.

Spectroscopic observations were carried out on 2008 December 28 and 29 with the Inter University Centre of Astronomy and Astrophysics (IUCAA) Girawali 2 m Telescope located at suburb of Pune, India. We used the IUCAA Faint Object Spectrograph and Camera (IFOSC). It has a 2048 $\times$ 2048 EEV CCD with a spatial scale of $0\farcs31$ pixel^{-1}. The IFOSC5 grism was used with a $1\farcs5$ slit, providing a wavelength coverage of 5200 Å – 10300 Å with a resolution of 14 Å. Weather was fine and stable for both observing nights. Seeing was $0\farcs6$ on Dec. 28 and $0\farcs9$ on Dec. 29. The exposure time for each source was between 300 s and 1800 s, depending on the source brightness. Two, three, or four exposures were taken for each object (Table 1). SAO 56475 (A2V) was observed for a correction of the effects of telluric absorption. Exposures of twilight were taken at the end of each night as flat frames.

The Image Reduction and Analysis Facility (IRAF) was used for data reduction. After the overscan and bias frame were subtracted, each frame was divided by the normalized R-band flat, then hot and bad pixels were removed. Strong fringe appears beyond $\sim 7000\mathring{A}$, which prevents us from producing accurate spectra in that wavelength region. The wavelength was determined with telluric oxygen absorption bands (6276 Å, 6867 Å, and 7594 Å) and the Hα

feature, either emission or absorption, in the object spectrum. Uncertainty in the wavelength calibration is 1.3 Å. Sky emission lines were suppressed by subtracting the counts in vicinity of the object's spectrum at each wavelength, with the BACKGROUND task. Individual spectra were extracted from the background subtracted images using the APALL task. The region where the intensity of the object was more than 10 % of the peak intensity at each wavelength was summed into a one-dimensional spectrum. The extracted spectra were then normalized and combined. The object spectra were divided by the standard star spectra, in which the Hα absorption line at 6563 Å was removed by interpolating across the adjacent continuum with the SPLOT task. Finally, the spectrum was multiplied by a blackbody spectrum of a temperature appropriate to the spectral type of the standard star (Tokunaga 2000).

3. Results and Discussion

The optical spectra of the 14 objects are shown in Figure 1. Prominent features in the spectra are the Hα emission at 6563 Å and broad molecular absorption bands, mainly due to TiO. We do not identify any forbidden emission lines. Equivalent widths of the Hα line were measured with the SPLOT task by Gaussian fitting (Table 2). Uncertainty in the equivalent width is estimated from the standard deviation of the adjacent continuum. We identified 11 objects as YSOs, whose Hα feature is in emission. Among the other objects, one object shows absorption and 2 objects do not show emission nor absorption at the Hα feature.

Oasa et al. (2008) classified the objects into 3 groups using near-infrared color-color diagram as given in Table 1. The objects classified as "Class III and field stars" do not have significant infrared excess. Weak-line T Tauri stars are categorized into this group. "Class II" objects are analogs to classical T Tauri stars. They show infrared excess arising from circumstellar disks. Objects intrinsically redder than the Class II objects are classified as "Class I" objects. Protostars deeply surrounded by circumstellar disks and envelopes are categorized into this group. It is generally thought that a stellar object evolves from the Class I stage through the Class II, to the Class III stage. Figure 2 shows Hα equivalent widths of the observed objects. The Class I objects have the largest equivalent widths, whereas the equivalent widths of the Class III objects are small. The Hα equivalent widths decreases as the objects evolve. This trend indicates that an accretion rate of the object decreases as it evolves at the pre-main sequence stage.

The spectral types of the objects are determined by comparing the overall shape of the spectra after reddening correction with the shape of template spectra. The template spectra of dwarfs and giants are taken from Pickles (1998). We also take those of very-late dwarfs ($>$ M6.5) from Kirkpatrick et al. (1999). For the Class III objects, the spectral types and the visual extinction are simultaneously determined. We measured the difference between the observed $J-H$ color and the intrinsic $J-H$ color of dwarfs or giants with the same spectral types. The $J-H$ colors of dwarfs and giants are taken from Tokunaga (2000), except for those of very-late

type dwarfs (>M8, Kirkpatrick et al. 2000). Then, the color difference are converted to amount of visual extinction. We used the extinction law of Cohen et al. (1981). We set $A_V = 0$, if the observed $J-H$ magnitude is smaller than those of dwarfs or giants. The A_V-corrected spectra are compared with the template spectra (see Figure 3 for an example). For the Class I objects and the Class II objects, the observed spectra are deredden with the visual extinctions, then spectral types are determined. The visual extinction of the Class II objects are estimated on the near-infrared color-color diagram (Itoh et al. 2002). For the Class I objects, we assume that the intrinsic near-infrared colors are extrapolated to those of the Class II objects. As a result, spectral types of all except three objects are determined as M-type (Table 2). Uncertainty in the spectral type is about 1 subclass. For Class I sources (OTSS 3 and 4), any template spectra do not match well to the object's spectra, especially in longer wavelengths. This mismatch may be caused by heavy veiling effect. All objects classified as M-types show the H_α line in emission. We confirmed that the YSO candidates previously identified as Class I and II objects (OTSS 1, 3, 4, and 12) by near-infrared excess are indeed YSOs. The other M-type objects which are not previously classified as YSO candidates due to lack of near-infrared excess also have the H_α emission. We consider that they are YSOs with little near-infrared excesses. In contrast, all objects not classified as M-type do not show the H_α line in emission. Two objects (OTSS 13 and 56) are identified as K-type and show neither emission nor absorption. One object (OTSS 16) is classified into F or G type and shows absorption at the H_α line. We identified this object as a background star. Oasa et al. (2008) found 76 objects in the central region of NGC 1333. Among them, 44 objects have near-infrared excesses, and the rest 32 objects do not show certain near-infrared excess in the JHK-bands. In this study, we detected the H_α emission line, indicative of youth, from 4 objects out of 7 M-type objects which do not show near-infrared excesses. Thus, we estimate that about half of the near-infrared objects without near-infrared excess are not background stars but indeed YSOs.

Spectral types of 11 objects were previously identified by near-infrared K-band spectra (Aspin 2003). Figure 4 shows spectral types determined in the optical wavelengths and those in the near-infrared wavelengths. For many objects, the optical spectral types tend to be later than the near-infrared spectral types. Some YSOs have heavy continuum veiling in the K-band, which weakens absorption lines and bands. Since molecular absorption bands are stronger for lower temperature and those are the most prominent indicators of spectral classification for low temperature objects, a low-mass object with heavy veiling in the K-band tends to be estimated as a higher temperature object. As a YSO often has continuum excess in near-infrared wavelengths due to its circumstellar disk, the near-infrared spectral type of a low-mass YSO may be estimated to be earlier than what it indeed is.

In order to place the objects on the HR diagram and to investigate their evolutionary stage, we estimated their photospheric luminosities and effective temperatures. The photospheric luminosity was derived from the J-band magnitude of the object. For YSOs, the

J-band emission arises primarily from the photosphere (Bertout et al. 1988). The estimate procedure is the same as that in Itoh et al. (2002); We calculated the extinction corrected absolute J-band magnitude, and the photospheric luminosities by comparing the absolute J-band magnitudes of very low-mass dwarfs (Leggett et al. 1996). The effective temperatures were derived from the spectral types of the objects. We calculated the lowest temperature from the dwarf spectral type. The conversion scale from the spectral types to the effective temperature for dwarfs (Tokunaga 2000) was used. For the latest dwarfs, we applied the scale presented in Bessell (1991). We also calculated the highest temperature from the giant spectral type with the conversion scale for giants (Tokunaga 2000). For the latest giants, the scale of Fluks et al. (1994) was applied. Figure 5 shows the HR diagram of the YSOs with the evolutionary track of Baraffe et al. (1998). Mass and age of each YSO are estimated and tabulated in Table 2. All YSOs have masses less than 0.6 $M_\odot$. OTSS 7 and OTSS 12 have masses less than 0.08 $M_\odot$, i.e. they are young brown dwarfs.

There is no clear correlation between ages of the objects and YSO's class. OTSS 3 and 4 are Class I objects, but unexpectedly old. Underestimates of the luminosity may lead such old age. We assumed that intrinsic color of Class I objects is extrapolation of the intrinsic color of Class II objects, but it is not well determined. If it is bluer in the $J-H$ color, A_V of the object increases, thus object's photospheric luminosity also increases. For example, if the intrinsic $J-H$ color is 0.5 mag, ages of the both objects are estimated to be less than 1 Myr. Otherwise, overestimates of the effective temperature may induce their old ages. If the temperatures are ~ 3100 K, the estimated ages of both objects are less than 1 Myr. This temperature corresponds to a spectral type of M4V or M7III. The spectral type of M4V is well considerable since both objects are assigned as M3V and the uncertainty is 1 subclass. On the other hand, an optical spectrum of an M7III object is very different from the observed spectra of OTSS 3 and 4.

OTSS 7 and ASR94-42 are Class III objects, but have very young ages. Since the NGC 1333 cluster is a dense cluster, circumstellar materials of the objects may be stripped by stellar encounters. Otherwise, overestimate of their luminosity may cause such young ages. Hirota et al. (2008) recently proposed the distance of the Perseus cloud to be 235 pc. With this distance, the ages of the both objects are estimated to be over 1 Myr. Also, the uncertainty in evolutionary tracks may cause this dissonance. If we use the tracks of D'Antona & Mazzitelli (1997), the age of OTSS 7 is estimated as 1 Myr. However, in the both cases, ages of all YSOs in this region also increase, which seem unplausible. Underestimate in their temperature may also produce their young age. If we adopt the temperatures estimated with the giant scale, the ages of the objects are 1 Myr.

Figure 6 shows the Hα emission line strengths as a function of the spectral types of the objects. One may find weak trend that the more massive objects have stronger emission. Note that late-spectral type dwarfs often show the Hα emission line of chromospheric origin. Further

investigations, such as detection of the Li absorption line by high resolution spectroscopy, are required for identification of their nature.

4. Conclusions

We have conducted low-resolution optical spectroscopy of 14 low-luminosity YSO candidates in the NGC 1333 cluster. Eleven targets have the Hα line in emission with M-type spectra, strongly indicating that they are indeed low-mass YSOs. Among them, two objects are young brown dwarfs. The YSOs with large amount of near-infrared excess show strong Hα emission. In the region, there are many fainter YSO candidates previously identified by the near-infrared imaging survey. They are not yet confirmed as YSOs by spectroscopy. Many of them may have less-massive YSOs, i.e. young brown dwarfs. The NGC 1333 cluster is known as the nearest star-forming region of intermediate mass stars. Our observation reveals that low-mass stars are forming in this region as well.

We are grateful for constructive and useful comments from an anonymous referee. This work is supported by "the Japan-India Cooperative Science Program" carried out by Japan Society for the Promotion of Science (JSPS) and the Department of Science and Technology (DST), Government of India. Y.I. is supported by a Grant-in-Aid for Scientific Research No. 19740276.

References

Aspin, C., Sandell, G., Russell, A. P. G., 1994, A&AS, 106, 165
Aspin, C., 2003, AJ, 125, 1480
Baraffe, I., et al. 1998, A&A, 337, 403
Bertout, C., Basri, G., Bouvier, J., 1988, ApJ, 330, 350
Bessell, M. S., 1991, AJ, 101, 662
Cohen, J. G. et al., 1981, ApJ, 249, 481
Comeron, F. et al., 1993, ApJ, 416, 185
D'Antona, F., Mazzitelli, I., 1997, Mem. Soc. Astron. Italiana, 68, 807
Fluks, M. A. et al., 1994, A&AS, 105, 311
Gutermuth, R. A. et al. 2008, ApJ, 674, 336
Hirota, T. et al., 2008, PASJ, 60, 37
Itoh, Y. et al., 1996, ApJ, 465, L129
Itoh, Y. et al., 2002, PASJ, 54, 561
Jayawardhana, R., Mohanty, S., Basri, G. 2003, ApJ, 592, 282
Kirkpatrick, J, D. et al., 1993, ApJ, 402, 643
Kirkpatrick, J, D. et al., 2000, AJ, 120, 447
Leggett, S. K. et al., 1996, ApJS, 104, 117
Luhman, K. L., et al. 2005, ApJ, 620, 51

Oasa, Y., et al. 1999, ApJ, 526, 336
Oasa, Y. et al., 2008, AJ, 136, 1372
Pickles, A. J., 1998, PASP, 110, 863
Tokunaga, A., 2000 in Astrophysical Quantities, ed. A.N. Cox (New York: AIP)
Whelan, E. T., et al. 2005, Nature, 435, 652
White, R. J., Basri, G., 2003, ApJ, 582, 1109
Winston, E. et al., 2009, AJ, 137, 4777

Table 1. Targets and observing log.

OTSS	ASR94	G08	YSO class	R-mag (ASR94)	Exposure
1	43	59	II	18.5	1500s × 2
3	107	61	I	19.7	1800s × 2
4	108	62	I	17.7	900s × 2
7	37		III	19.2	1800s × 3
12	15		II	21.2	1800s × 4
13	118	67	III	18.2	900s × 2
16	130		III	9.1	1800s × 3
21	36		III	16.9	600s × 2
32	3	76	III	17.9	900s × 2
35	2		III	15.6	600s × 2
40	8		III	18.0	400s × 2
56	56		III	14.4	300s × 2
	46	55	III	18.2	900s × 2
	42	58	III	18.6	1500s × 2

OTSS: Oasa et al. (2008)

G08: Gutermuth et al. (2008)

ASR94: Aspin et al. (1994)

Table 2. Equivalent widths of the Hα line and derived stellar parameters

OTSS	ASR94	EW(Hα) [Å]	A_V [mag]	Sp type Dwarf	Sp type Giant	Sp type A03	Sp type W09	Mass [M$\odot$]	Age [Myr]
1	43	-45.7 ± 0.2	4.1	M2V	M3III	O6-9V	M1.0±1.5	0.6	1.6
3	107	-33.1 ± 2.0	1.9	M3V	M4III			0.4	7
4	108	-211 ± 1	0.8	M3V	M4III		M0.5±1.5	0.4	3
7	37	-3.6 ± 0.9	1.1	M6.5V	M7III	B6-9V		0.08	<1
12	15	-3.6 ± 1.3	0.7	M6.5V	M7III	O-BV		0.06	4
13	118	cont.	10	KV	K5-M2III	K0-4	M3.5±1.0	1.3	5
16	130	$+2.8 \pm 0.4$		F-G		A6-9V			
21	36	-4.4 ± 0.4	3.2	M2V	M2III	K3-6V		0.6	3
32	3	-3.3 ± 0.3	0	M4.5V	M5III	K0-3V		0.2	13
35	2	-2.3 ± 0.2	0.3	M4V	M4III	K0-3V		0.3	5
40	8	-8.7 ± 0.3	0	M6V	M6III	O3-9V		0.12	1
56	56	cont.		KV		K0-3V			
	46	-10.0 ± 0.7	0.6	M6V	M6III		M5.0±1.0	0.12	1
	42	-18.2 ± 0.6	3.4	M5V	M6III	G6-9V	M5.0±1.0	0.15	<1

A03: Aspin (2003)

W09: Winston et al. (2009)

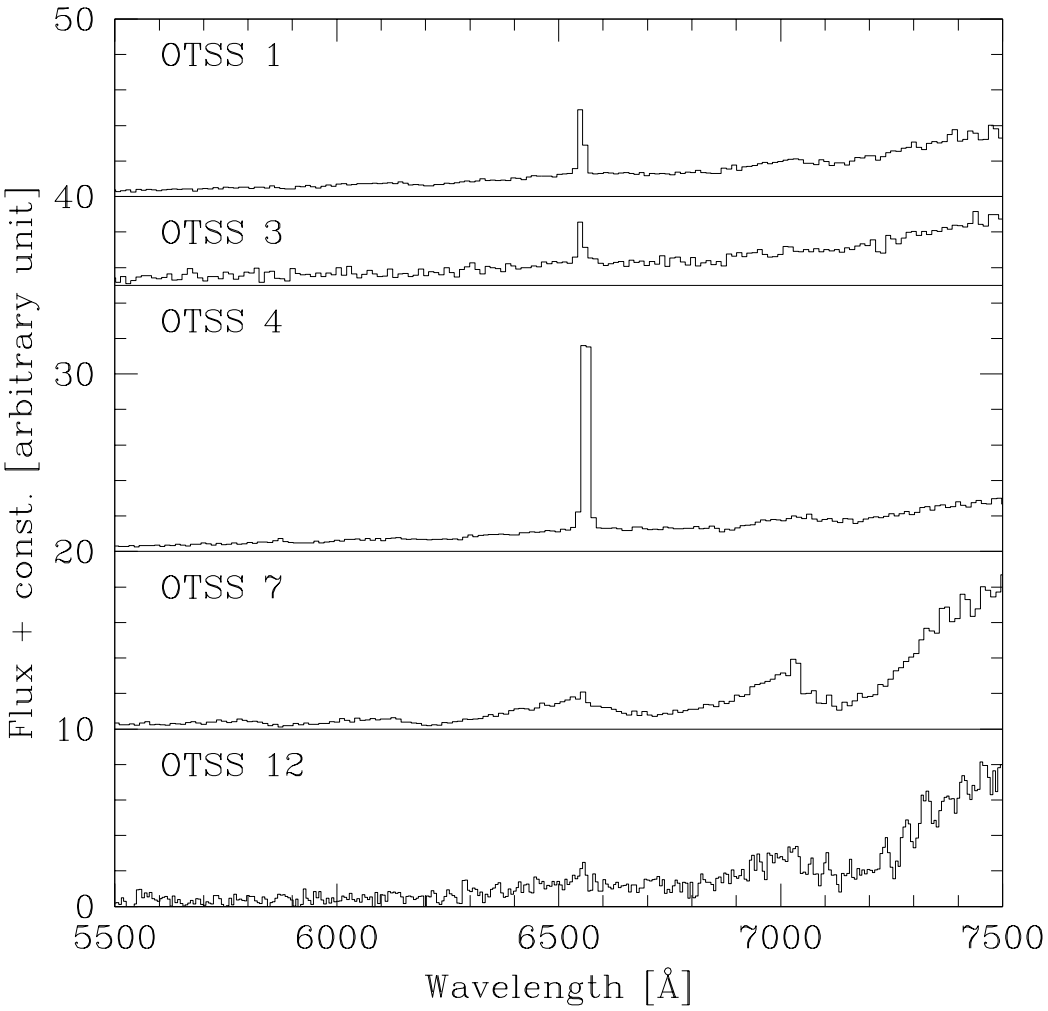

Fig. 1. (a) Optical spectra of the YSO candidates in NGC 1333. The spectra are normalized between 6350 Å and 6450 Å.

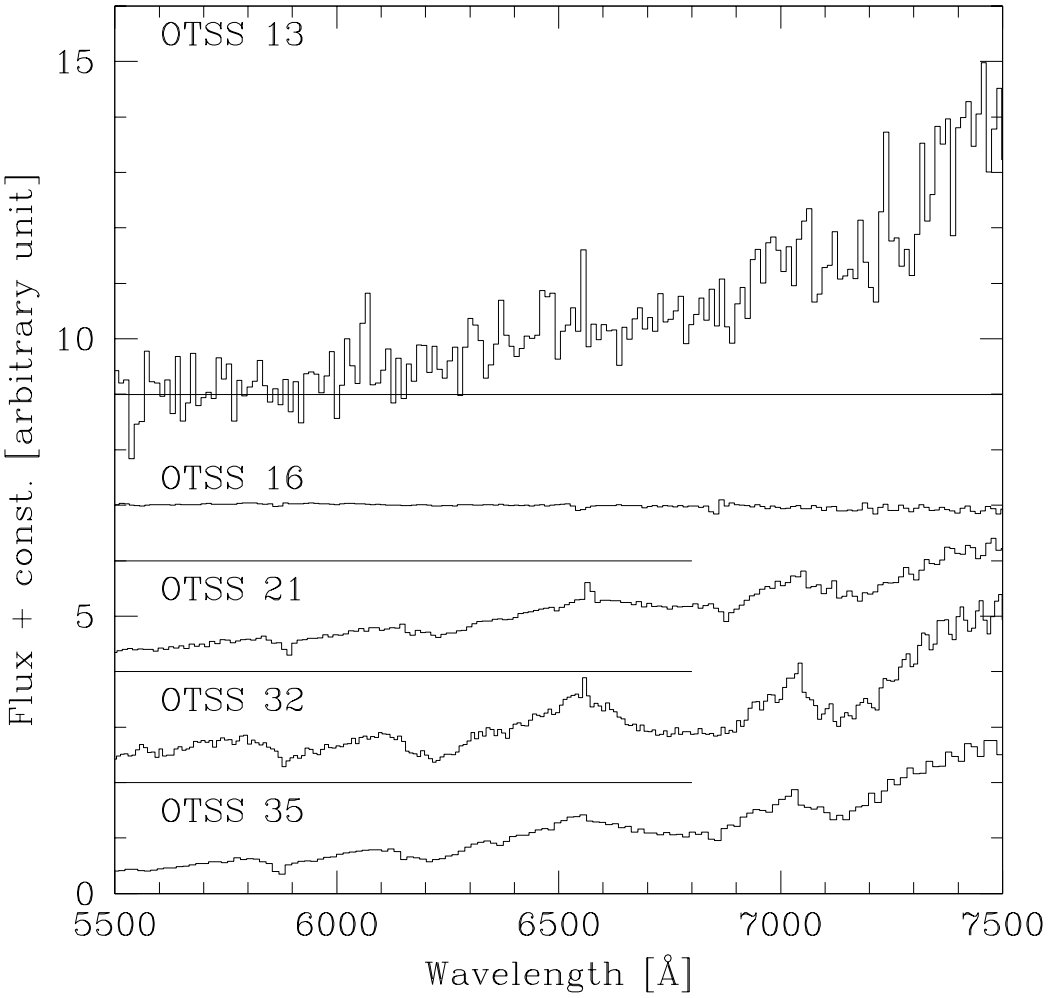

Fig. 1. (b) Optical spectra of the YSO candidates in NGC 1333.

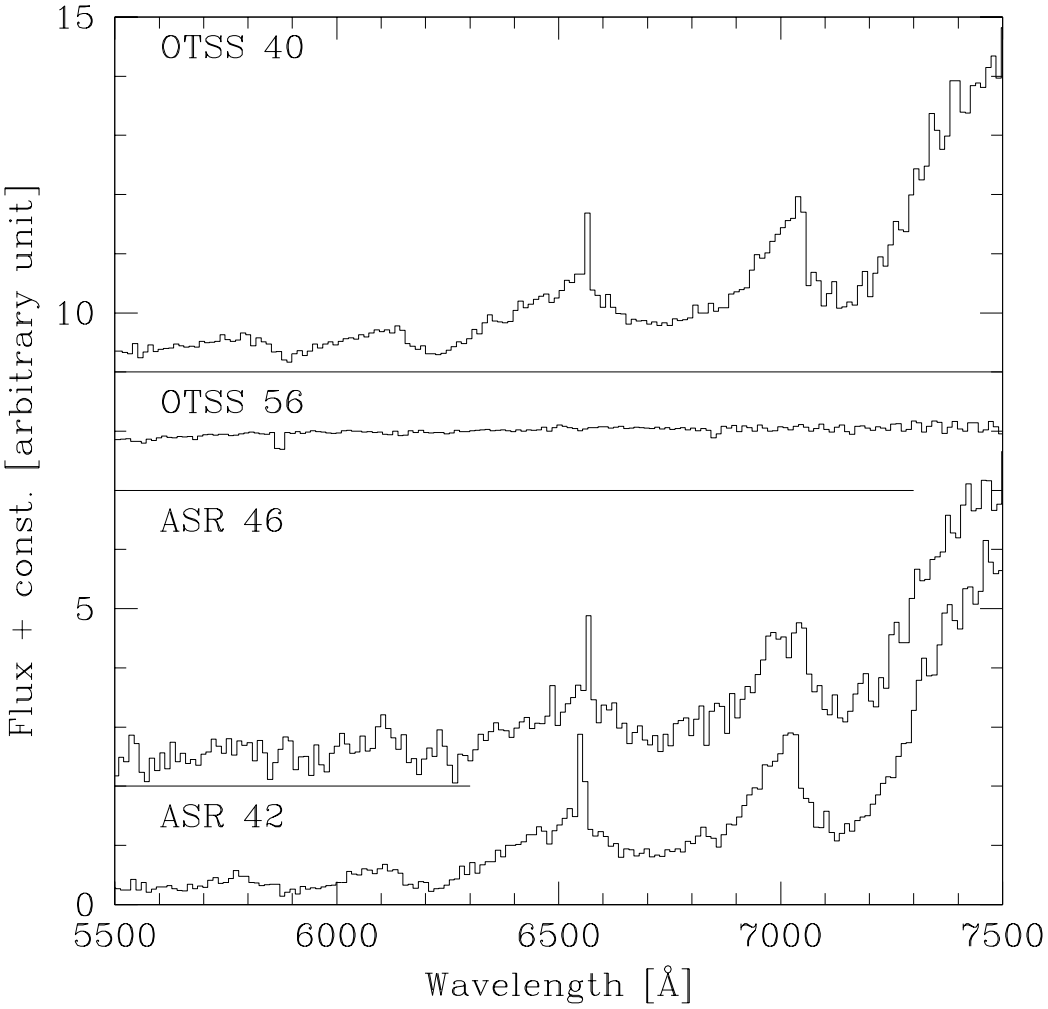

Fig. 1. (c) Optical spectra of the YSO candidates in NGC 1333.

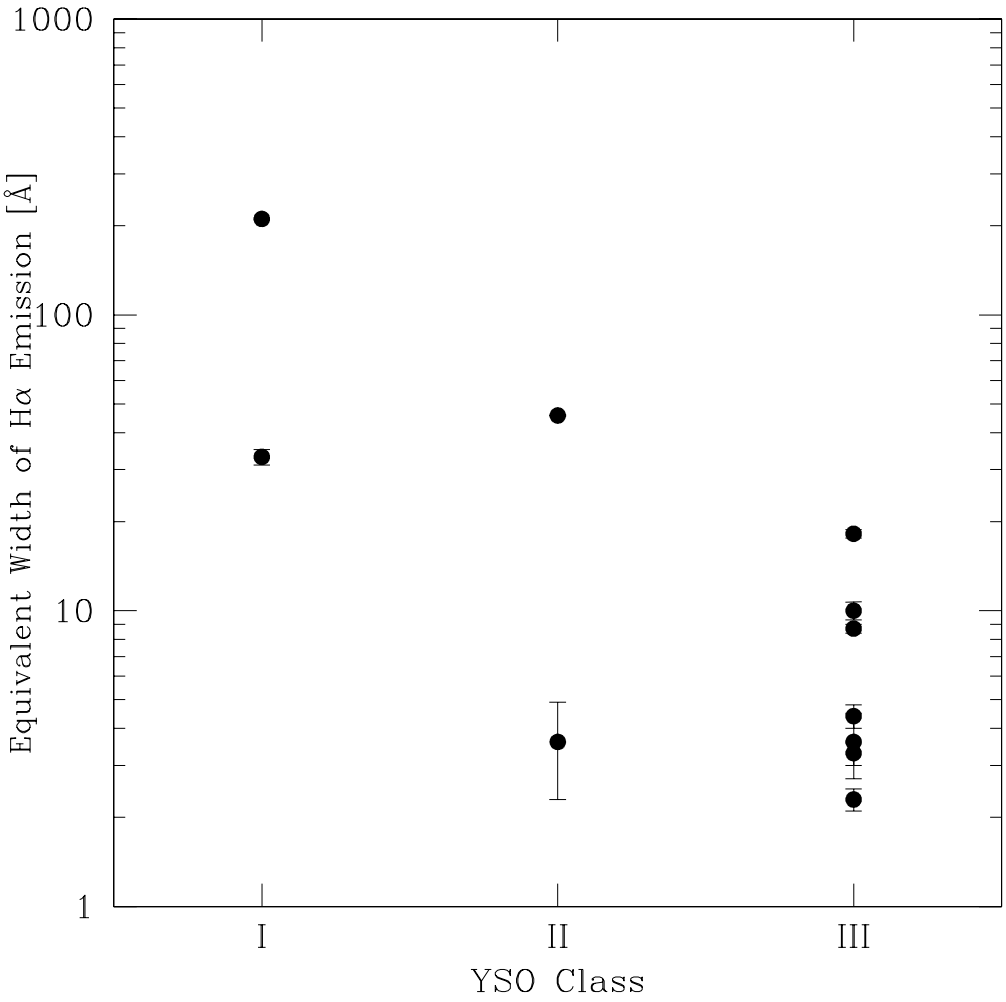

Fig. 2. Strengths of the Hα emission line and the YSO class. The younger objects show the stronger emission line.

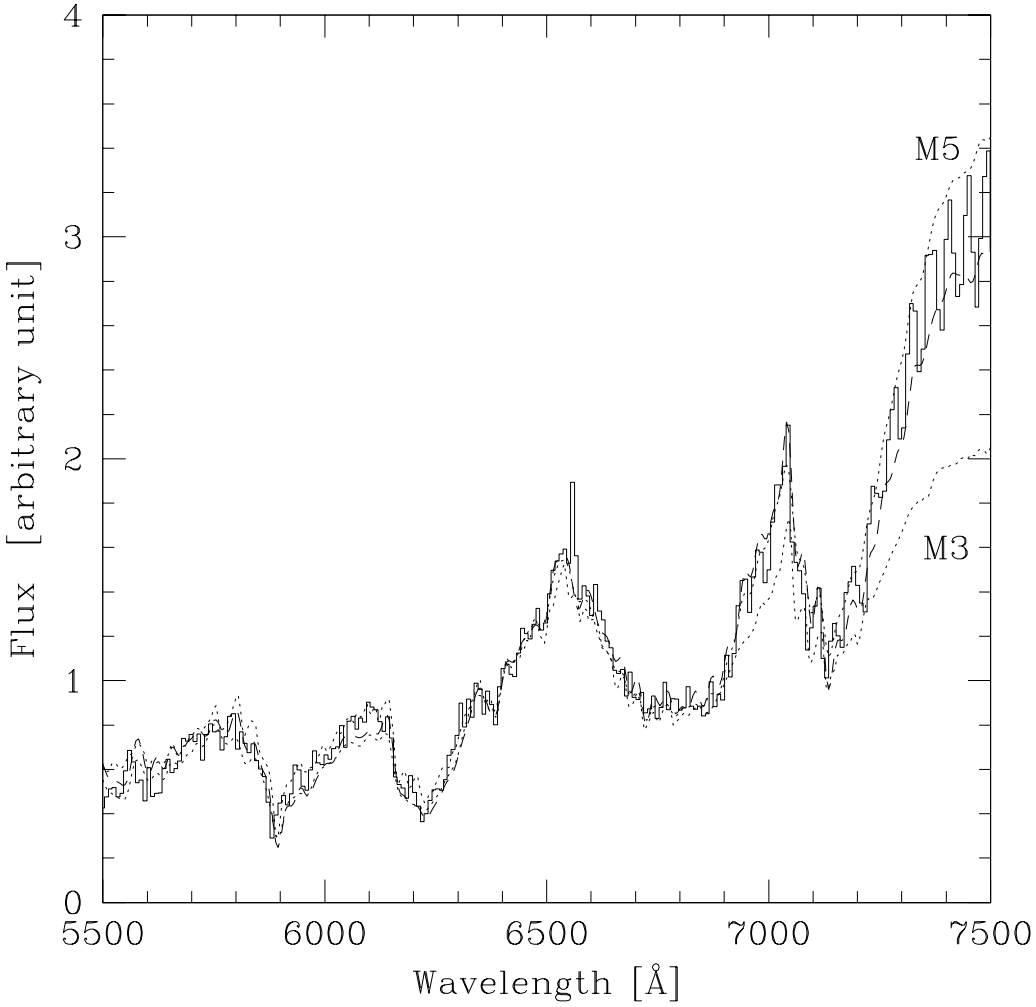

Fig. 3. An optical spectrum of OTSS 32 (the solid line), with template spectra of an M4 dwarfs (the dashed line) and M3 and M5 dwarfs (the dotted lines). By comparing these spectra, we classified the spectral type of OTSS 32 as M4.5V.

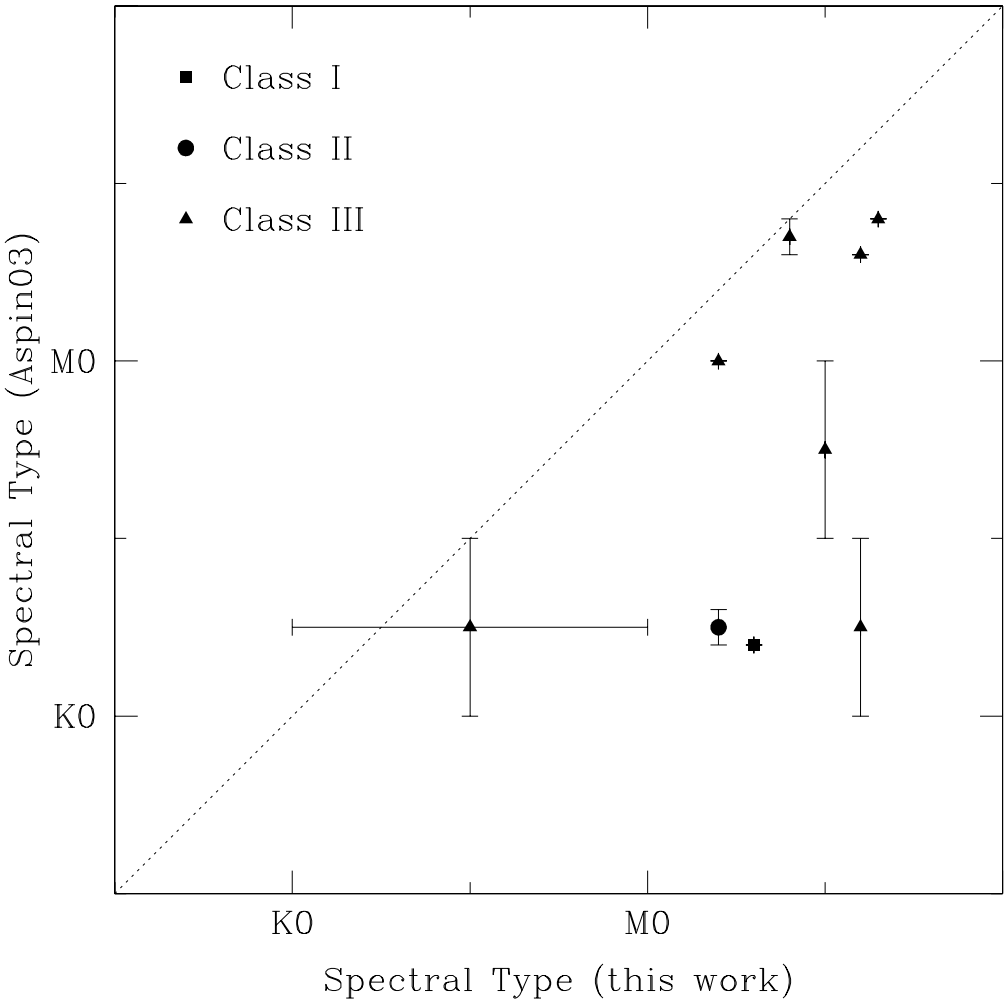

Fig. 4. Comparison of the derived optical spectral types of the YSO candidates with the near-infrared spectral types quoted by Aspin et al. (2003). The spectral types in the dwarf scale are presented in both axes.

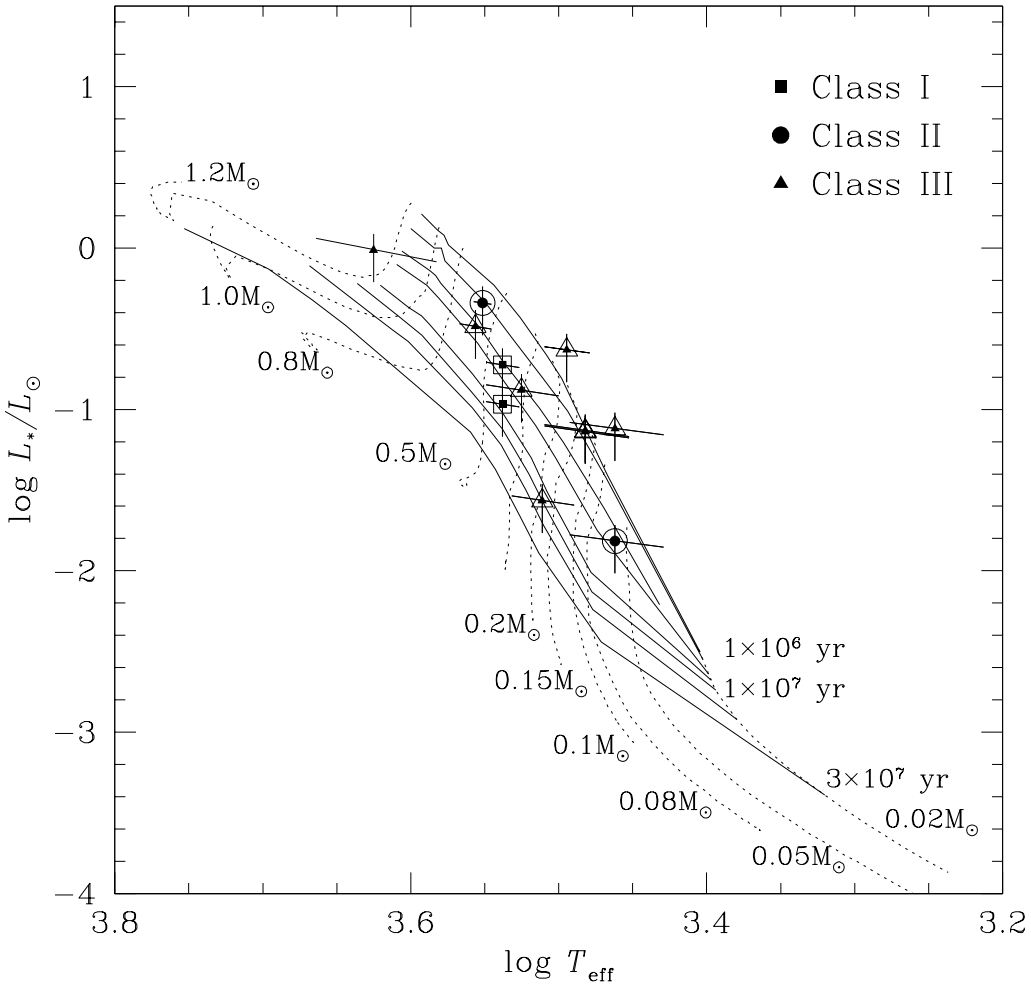

Fig. 5. HR diagram of the YSO candidates. The Class I objects are shown by the filled squares, Class II by the filled circles, and Class III by the filled triangles. The objects with the Hα line in emission are encircled by large symbols. Evolutionary tracks and isochrones of Baraffe et al. (1998) are also shown.

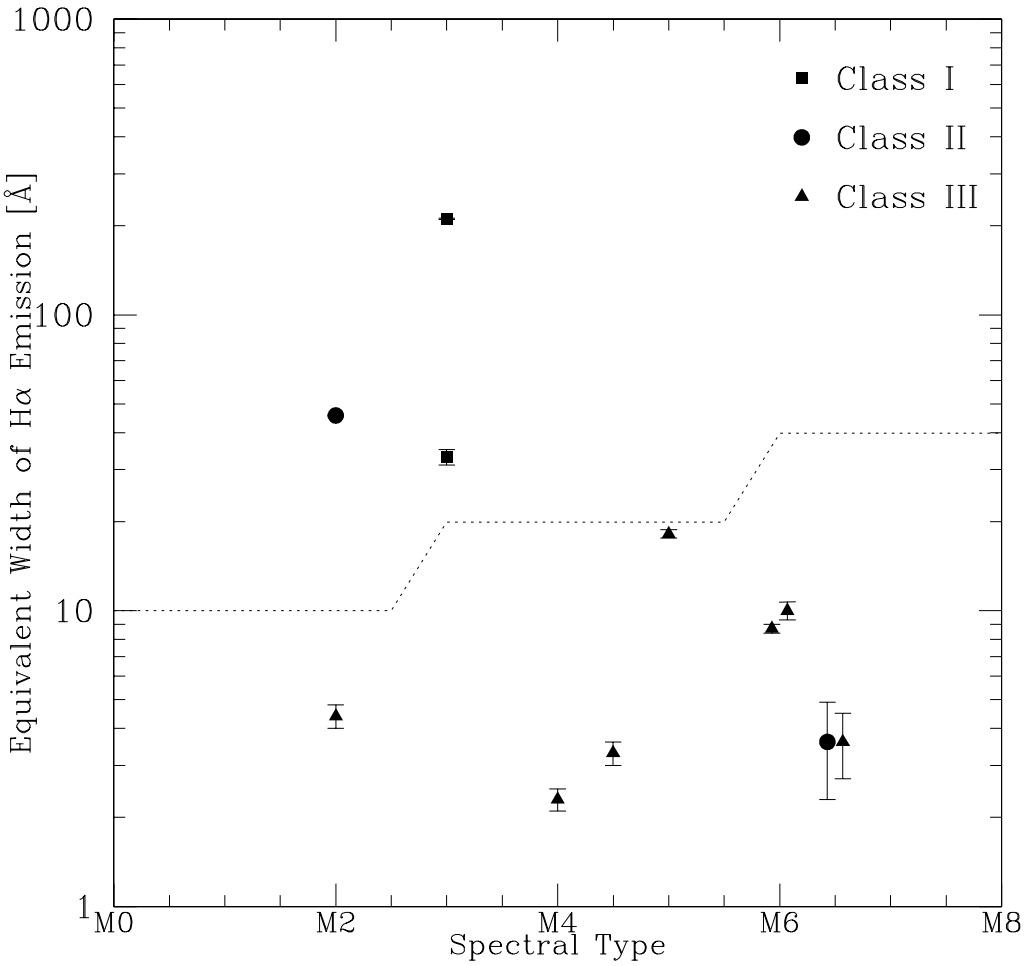

Fig. 6. The Hα emission strengths as a function of the dwarf spectral types of the YSOs. The dotted line indicates border of classical T Tauri stars and weak-line T Tauri stars (White & Basri 2003).